OPTICS

Observation of Anderson localization beyond the spectrum of the disorder

Alex Dikopoltsev[1]†, Sebastian Weidemann[2]†, Mark Kremer[2]†, Andrea Steinfurth[2], Hanan Herzig Sheinfux[1,3], Alexander Szameit[2]*, Mordechai Segev[1,4]

Anderson localization predicts that transport in one-dimensional uncorrelated disordered systems comes to a complete halt, experiencing no transport whatsoever. However, in reality, a disordered physical system is always correlated because it must have a finite spectrum. Common wisdom in the field states that localization is dominant only for wave packets whose spectral extent resides within the region of the wave number span of the disorder. Here, we show experimentally that Anderson localization can occur and even be dominant for wave packets residing entirely outside the spectral extent of the disorder. We study the evolution of wave packets in synthetic photonic lattices containing bandwidth-limited (correlated) disorder and observe strong localization for wave packets centered at twice the mean wave number of the disorder spectral extent and at low wave numbers, both far beyond the spectrum of the disorder. Our results shed light on fundamental aspects of disordered systems and offer avenues for using spectrally shaped disorder for controlling transport.

INTRODUCTION

It has been known for two millennia that particles experience stochastic motion while falling through voids (*1*), which was later understood as diffusive motion due to random walk. After the discovery of the electron, P. Drude (*2*) showed that the random walk of electrons is at the heart of electrical conduction, giving rise to Ohm's law. It came as a surprise when, half a century later, P. W. Anderson (*3*) argued that the wave nature of electrons plays a crucial role in their dynamics in random media and predicted that interference effects can bring all transport to a complete halt. This phenomenon of Anderson localization requires the potential to be stationary and the absence of interactions. However, electrons inevitably interact with one another; hence, Anderson localization of electrons in solids remained elusive. Nevertheless, almost four decades ago, it was realized that localization is a universal wave phenomenon (*4*–*7*) and since then was demonstrated in a variety of systems, ranging from light scattering in dielectric media (*8*–*10*), microwaves (*11*, *12*), and disordered photonic lattices (*13*–*15*) to sound waves (*16*) and cold atoms (*17*, *18*). The study of waves in disordered media and localization is an extremely rich field, generating unexpected previously unknown phenomena such as Levy flight (*19*), hyper-transport (*20*), localization by deep subwavelength disorder (*21*), and localization phenomena in unusual settings such as amorphous media (*22*, *23*), Moire lattices (*24*), and non-Hermitian systems (*25*).

The propagation of waves in random media is characterized by localized eigenstates with exponentially decaying tails such that their ensemble average, taken over multiple realizations of the disorder, yields a measure called the localization length, l_{loc}, equal to the inverse of the decay rate of the ensemble-averaged wave function. Using a universal model, it was predicted that in infinite one-dimensional (1D) or 2D systems with uncorrelated disorder, all eigenstates become exponentially localized (*26*, *27*). The outcome of the process, whether the system supports transport or not, is different for finite systems, where some eigenstates have l_{loc} larger than the system size L. These modes can facilitate transport in finite systems and are typically termed extended (*28*, *29*), whereas the modes with l_{loc} substantially smaller than L are considered localized and do not support transport. Moreover, l_{loc} depends on the spectrum of the disorder, and therefore, spatially correlated systems can display spectrally dependent transport. Essentially, the spectrum of the disorder in a physical system always has a finite extent, determined by the smallest length scale in the system. This implies that any disorder in physical systems is always correlated in space (through simple Fourier relations). The spectral extent of the disorder sets bounds on l_{loc}, which directly depends on the spatial correlations of the disorder. For example, it has been shown that correlations in 1D systems can induce a mobility edge (*29*). It is therefore instructive to consider localization from a spectral perspective.

Consider a 1D system with a disordered potential $V(x)$. This system may have a real dimension x like when light propagates in a 1D lattice of waveguides (*30*, *31*) or a synthetic dimension, where the dynamics occurs in the modal space (*32*) or time-bin–encoded lattices (*33*). The spatial power spectrum of the disorder $S(k) \propto |\mathrm{FT}\{V(x)\}|^2$ is the Fourier transform (FT) of the two-point correlation function of the potential, $C_V(x, x')$, and it determines the range of possible scattering processes allowed by the momentum exchanges between the waves and the disordered potential (Fig. 1A) (*28*, *34*, *35*). One may think of the localization phenomenon as the outcome of multiple scattering processes of waves from the disordered potential, where the disorder is constructed as an ensemble of random gratings whose wave numbers define $S(k)$ (*36*). Every spectral component of the disorder behaves as a diffraction grating that scatters one plane wave component into another, which is essentially a transition between different wave vectors. The primary scattering process of a plane wave is mediated by only a single spectral component of the disorder, similar to a Bragg reflection off a grating with a spectral component k. In this picture, multiple transitions of these first-order scattering events from a collection of gratings with random amplitudes and phases (constituting the

[1]Physics Department, Technion, 32000 Haifa, Israel. [2]Institute for Physics, University of Rostock, 18059 Rostock, Germany. [3]ICFO-Institute of Photonic Sciences, Mediterranean Technology Park, 08860 Castelldefels, Barcelona, Spain. [4]Electrical Engineering Department, Technion, 32000 Haifa, Israel.
*Corresponding author. Email: alexander.szameit@uni-rostock.de
†These authors contributed equally to this work.

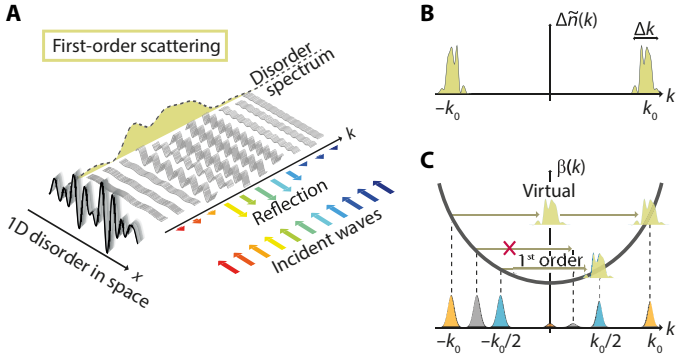

Fig. 1. Localization through spectrally dependent scattering and transitions. (**A**) Localization via first-order scattering: waves with different wave numbers k (different colors) undergo scattering events that depend on the spectral decomposition of the potential. (**B**) The bandwidth-limited spectrum of correlated disorder, $\Delta\tilde{n}(k)$, represents gratings with random amplitude and phase. The nonzero components lie in the intervals $[\pm k_0 - \Delta k/2, \pm k_0 + \Delta k/2]$. (**C**) Scattering processes mediated by a single spectral component k_0 [from $\Delta\tilde{n}(k)$], with the dispersion curve $\beta(k) = k^2/2\beta$ describing the phase mismatch. A first-order phase-matched transition: A wave of wave number $-k_0/2$ scatters efficiently to $k_0/2$ because $\beta(-k_0/2) = \beta(k_0/2)$. A second-order phase-matched transition takes place when a wave scatters from $-k_0$ to 0 and subsequently to k_0. The intermediate state at $k = 0$ is called virtual because it is phase mismatched with the initial wave $\beta(-k_0)$ unequal to $\beta(0)$. With the grating component at $\pm k_0$, there is no phase-matched scattering for a wave that starts with $-0.75k_0$.

disordered system) may bring transport to a halt, giving rise to Anderson localization (*36*).

Accordingly, for localization mediated by first-order transitions, the localization length l_{loc} is inversely proportional to the mean amplitude of the power spectrum of the disorder $S(k)$ (*37*). Following this reasoning, it seemed, for some time, that localization in systems with correlated disorder can occur only for wave packets whose spectrum is fully contained within the spectral extent of the disorder (*12*, *17*, *28*, *38*). However, it was later found that localization can also be induced by two (or more) consecutive contributions of the potential (*37*, *39*, *40*), which may lead to localization outside the spectral extent of $S(k)$. We henceforth refer to the scattering processes involving intermediate wave numbers outside the spectrum of the disorder as "virtual," in analogy (explained later) to atomic transitions through a virtual energy level. In general, these second-order processes are significantly weaker than first-order transitions. Consequently, thus far, in all experiments showing Anderson localization in all fields of science, the main contribution came from "first-order" transitions. Therefore, experimentally, Anderson localization was always limited to the spectral reach of the disorder (*8*, *10*–*14*, *16*–*18*).

Here, we observe Anderson localization for wave packets residing entirely outside the spectral extent of the disorder, mitigated solely by virtual transitions. Our experiments are carried out in synthetic photonic lattices containing bandwidth-limited disorder and demonstrate how virtual (two-step) transitions lead to Anderson localization around twice the mean wave number of the spectral extent of the disorder. In addition, we predict and observe universal localization at low wave numbers, implying that any low–wave number wave packet can strongly localize even when the disorder is strictly at high wave numbers. The underlying mechanism requires only for the spectrum of the disorder to be symmetric, irrespective of its spectral shape. The symmetric transitions, which are natural to any Hermitian system, induce scattering to virtual states and back and eventually lead to very short localization lengths for low wave number wave packets.

RESULTS

We begin by explaining the underlying concepts using the transverse localization scheme (*7*, *13*) as a convenient example to frame the discussion. This scheme exploits the mathematical equivalence between the paraxial wave equation for light and the Schrödinger equation (see the first section of the Supplementary Materials). This equivalence has been used to experimentally observe a plethora of wave phenomena, such as Floquet topological insulators (*41*), bound states in the continuum (*42*), topological Anderson insulators (*43*), and Anderson localization in a lattice containing disorder (*13*). The paraxial wave equation for the slowly varying amplitude of the light propagating in a 2D dielectric medium is

$$i\frac{\partial\psi(x,z)}{\partial z} = -\frac{1}{2\beta_0}\frac{\partial^2}{\partial x^2}\psi(x,z) - \frac{\beta_0}{n_0}\Delta n(x)\,\psi(x,z) \qquad (1)$$

where $\beta_0 = \omega n_0/c$ is the wave number, z is the propagation direction (analogous to time in the Schrödinger equation), x is the transverse coordinate, n_0 is the ambient refractive index, and $\Delta n(x)$ is the local perturbation on n_0 acting as a random potential. We are specifically interested in Δn that does not depend on the evolution coordinate z and, hence, can cause localization (*13*). From the linearity of the equations, $\Delta n(x)$ can be written as a superposition of periodic functions, such as $\sin(kx + \phi_k)$ (see section S2 in the Supplementary Materials), where k is the spatial frequency, and ϕ_k is the phase, each acting as a grating component causing the spectral components of $\psi(x, z)$ to experience diffraction off this grating (Fig. 1A). In this system, wave functions $\psi(x, z)$, composed of wave components with transverse wave numbers within the spectral extent of the disorder, can become localized after some finite propagation distance (*7*, *13*, *14*, *31*). The evolution of a wave packet in k-space is defined by the spatial FT of Eq. 1

$$i\frac{\partial\tilde{\psi}(k,z)}{\partial z} = \frac{1}{2\beta_0}k^2\tilde{\psi}(k,z) - \frac{\beta_0}{n_0}\int\Delta\tilde{n}(k')\,\tilde{\psi}(k-k',z)\,dk' \qquad (2)$$

where $\tilde{\psi}(k,z)$ and $\Delta\tilde{n}(k)$ are the transverse FT of $\psi(x, z)$ and $\Delta n(x)$, respectively, and k is the transverse wave number (where $k \ll \beta_0$). We can treat plane waves as eigenstates of a spatially homogeneous system, with the disorder coupling between them by convolutions (right hand side of Eq. 2) with components in the spectrum of the disorder. These transitions in momentum space are naturally described by coupled-mode formalism (*44*). The coupling between two different plane waves can occur if the potential contains a suitable disorder component that can momentum-match between the incident and scattered waves (Fig. 1A). Using this coupled-mode formalism is fully equivalent to solving Eq. 1 in real space, and it is regularly used in analyzing wave phenomena. It relies on phase-matched interactions, which, in the analogous Schrödinger equation, represent transitions that conserve energy.

Consider first a disordered potential $\Delta n(x)$ such that its spectrum $\Delta\tilde{n}(k)$ consists of two regions in momentum space, with random amplitude and phase (Fig. 1B). Let us assume that spectral regions of the disorder are nonzero only in a small region Δk around wave

numbers $\pm k_0$. When $\Delta n(x)$ is real (as in our optical experiments, where the photonic system is Hermitian), $|\Delta\tilde{n}(k)|$ is symmetric. For a plane wave incident upon this potential with transverse wave number $k_{in} \approx -k_0/2$, there are many possible phase-matched first-order transitions to the spectral region around $k_0/2$, obeying the paraxial dispersion relation $\beta(k_{in}) = \beta(k_0/2)$, where $\beta(k) = \beta_0 - k^2/2\beta_0$ is the wave vector component in z (see the first section of the Supplementary Materials). This plane wave undergoes many sequential first-order transitions, from positive to negative wave numbers and back, leading to the buildup of Anderson localization (*36*). In this process, the spectrum of the localized wave packet reshapes but remains confined around $\pm k_0/2$.

However, our primary interest here are plane waves for which no phase-matched first-order transitions exist, and hence, only second-order transitions can contribute to localization. For an incident wave with transverse wave number $k_{in} \approx -k_0$, the first-order transitions in the bandwidth-limited potential of Fig. 1B, namely, $-k_0 \xrightarrow{-k_0} -2k_0$ and $-k_0 \xrightarrow{+k_0} 0$, are not phase matched. However, the two-step transition $-k_0 \xrightarrow{+k_0} 0 \xrightarrow{+k_0} k_0$ is in fact phase matched. We call the sequential transition virtual because energy does not accumulate in the intermediate state at $k = 0$ (Fig. 1C), in similarity to the role played by virtual levels in atomic systems where an electron can absorb two photons for a single atomic transition. Another possible virtual transition is from $k_{in} \approx 0$ to k_0 and back to $k = 0$, which is analogous to Kerr nonlinearity, where an electron is excited to a virtual level and back, while changing the refractive index in the process. These transitions require two scattering events mediated by two spectral components (two random gratings), which may have the same or different transverse wave numbers, as long as both gratings have nonzero amplitudes, i.e., they are both contained within the spectral extent of the correlated disorder (*40*).

To study the process of localization driven by spectrally shaped disorder, we investigate the evolution of wave packets with different initial transverse wave numbers $k_{in} \in [0,1.25k_0]$ in our system with bandwidth-limited disorder centered on k_0 with bandwidth $0.25k_0$ (Fig. 2). The creation of the bandwidth-limited disorder is explained in the second section of the Supplementary Materials. To describe the physics of random processes, statistical tools are required, and hence, meaningful results are obtained from ensemble averaging over multiple realizations of the disorder (*13*, *31*) (see the third section in the Supplementary Materials). Figure 2A shows the propagation of the ensemble-averaged wave packets in a system with bandwidth-limited disorder. At $k_{in} = 0$, the wave packet evolves without expanding, due to second-order processes. In the absence of disorder (i.e., in a homogeneous medium), the same input wave packet expands in width by ~5 times for the same propagation distance. Thus, the absence of diffraction broadening due to disorder is a clear and direct evidence for localization by two-step processes. At $k_{in} = 0.25k_0$, the wave packet is within the spectral extent of the strong disorder; hence, the wave packet shows feature of localization due to a bandwidth increase. It is a direct result of a strong disorder level, which increases the spectral extent of the localized eigenmodes around $0.5k_0$ beyond the range defined solely by the shape of the spectrum (see detailed explanation on that phenomenon in the fourth section of the Supplementary Materials). For $k_{in} = k_0/2$, multiple first-order transitions are phase matched; hence, the wave packet is localized: Its expansion stops, and it propagates on axis despite its initial momentum. This case is the ordinary outcome of Anderson localization. On the other hand, for $k_{in} = 0.83k_0$, the transitions are phase mismatched, so the wave packet expands as if it is unaffected by the disorder and propagates at its initial trajectory. When $k_{in} = k_0$, we again find evolution in the regime of second-order localization. Initially, the wave packet expands, but after some distance, the expansion stops, and the propagation remains on axis. The lack of expansion and the on-axis propagation show that this case is again localization by two-step processes. For $k_{in} = 1.25k_0$, the transitions are again phase mismatched, so the wave packet is (again) unaffected by the disorder: It expands and continues on its initial trajectory.

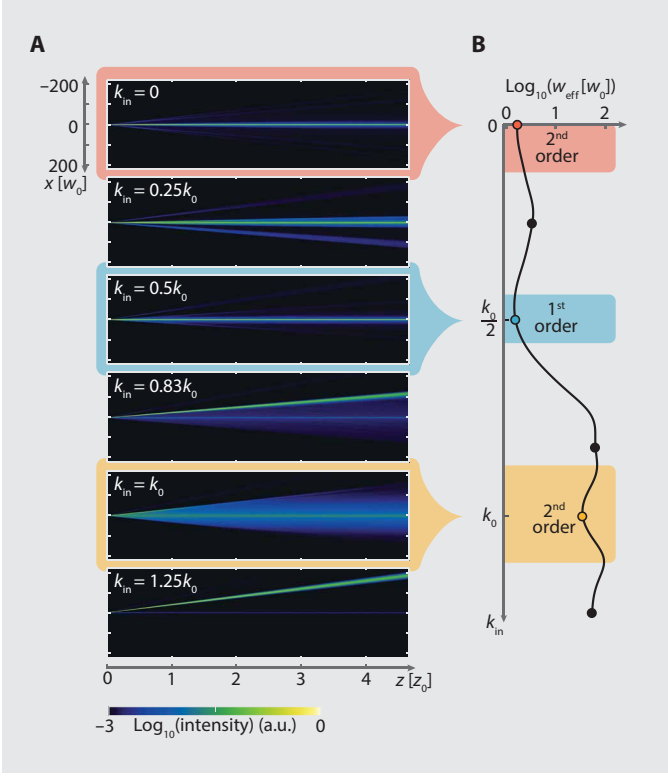

Fig. 2. Simulated first-order and second-order localization under correlated disorder. (**A**) Ensemble-averaged propagation taken over 100 disorder realizations, governed by Eq. 1, in an idealized system with bandwidth-limited disorder, all contained within a Δk region centered on $\pm k_0$. The input beam is a Gaussian wave packet launched at chosen initial momenta corresponding to different wave number (k_{in}) values. At $k_{in} = 0$, the natural diffraction broadening is arrested due to a second-order process. At $k_{in} = 0.25k_0$, the wave packet is within the extended spectral extent of the strong correlated disorder and therefore localizes. For $k_{in} = k_0/2$, localization occurs due to phase-matched first-order transitions. On the other hand, for $k_{in} = 0.83k_0$ and $k_{in} = 1.25k_0$, all transitions are phase mismatched, so the wave packet evolves almost unaffected by the disorder. When $k_{in} = k_0$, second-order processes induce localization. Initially, the wave packet expands, but after some distance, the expansion stops. We use normalized units for x and z (with the initial beam width w_0 and the Rayleigh length z_0, respectively). (**B**) Effective width of wave packets after propagation. The dip in the effective width indicating localization occurs in three regions: first-order localization (blue) and localization due to second-order transitions (red and orange). Notice three local minima in the effective widths at $k_{in} = 0$, $k_0/2$, and k_0 (see Supplementary Materials for parameters). a.u., arbitrary units.

The most important signature of a localized wave packet is the asymptotic halt of its expansion. To quantify the width of the wave packets and compare the expansion for different angles, we use the effective width, w_{eff} (*13*, *41*), which is the width of the ensemble-averaged

wave function of the intensity, with the ensemble taken over many realizations of the disorder of the same characteristics (power spectrum, average amplitude, etc.). For a 1D exponentially decaying function, w_{eff} is linearly proportional to its localization length l_{loc}. Figure 2B shows the effective width w_{eff} for several initial momenta. We mark the regions where w_{eff} is reduced by the scattering process (indicative for localization) and divide them into two types: (i) a region driven by first-order transitions (blue), where we find a local minimum around $k_{\mathrm{in}} = k_0/2$, and (ii) regions where only second-order processes dominate, where we find local minima in w_{eff} at $k_{\mathrm{in}} = 0$ (red) and k_0 (orange). The low effective width at $k_{\mathrm{in}} = k_0$ is a direct result of strictly second-order localization processes. The very low w_{eff} at low wave numbers (k_{in}~0) implies that, although second-order processes are generally weak, wave packets with low group velocities can be localized, with localization as strong as first-order localization. These simulations indicate that wave packets with wave number k_0, which are outside of the immediate influence zone of the potential, can indeed become localized. Together, as shown in Fig. 2, these multiple scattering processes induce Anderson localization by virtual transitions, with the localized wave packets residing completely outside the spectral extent of the disorder, specifically at twice the first-order localization wave numbers and also at very low wave numbers at the vicinity of zero.

To experimentally demonstrate Anderson localization strictly by second-order scattering, we use a synthetic 1D photonic lattice encoded in a time-bin system based on the propagation of light in coupled optical fiber loops (*33*, *46*, *47*). The implementation is based on the idea that the dynamics in the 1 + 1D double-discrete lattice (Fig. 3A), which is similar to the quantum walk of a single particle, describes the propagation of light pulses in coupled optical fiber loops (Fig. 3C). The corresponding mapping between the propagation of light and the evolution in the synthetic lattice is explained in the fifth section of the Supplementary Materials. The precisely tunable optical system makes it possible to create a multitude of photonic lattices, especially lattices with correlated disorder. This experimental setting allows to measure the squared modulus of the wave function at all steps of the evolution, such that one can obtain the full dynamics. These fiber-loop photonic lattices have proven to be powerful for experiments on numerous phenomena, such as Bloch oscillations and solitons in PT-symmetric systems (*46*–*49*), topological lattices (*50*), and even topological funneling of light (*51*).

The recursive equations describing the dynamics in our synthetic lattice are

$$\begin{aligned} u_n^{m+1} &= \frac{1}{\sqrt{2}}(u_{n+1}^m + i\,v_{n+1}^m)\,e^{i\varphi_u(n,m)} \\ v_n^{m+1} &= \frac{1}{\sqrt{2}}(i\,u_{n-1}^m + v_{n-1}^m) \end{aligned} \tag{3}$$

where u_n^m, v_n^m are the complex amplitudes of the pulses, corresponding to the wave function, at position (time-bin) n and time step m, in the short and long fiber loop, respectively. The parameters of this time-bin system can be adjusted to correspond to the localization phenomena described by Eq. 1. Specifically, in our system, we construct the real propagation-invariant potential, $\Delta n(x)$, by introducing phase modulation $\varphi_u = \varphi_u(n, m)$ in the u loop (*33*). Hence, through the phase modulation φ_u, we shape the disorder at will and control its spectral properties. To evaluate the ensemble average characteristics, it is sufficient to consider the intensity distribution in one of

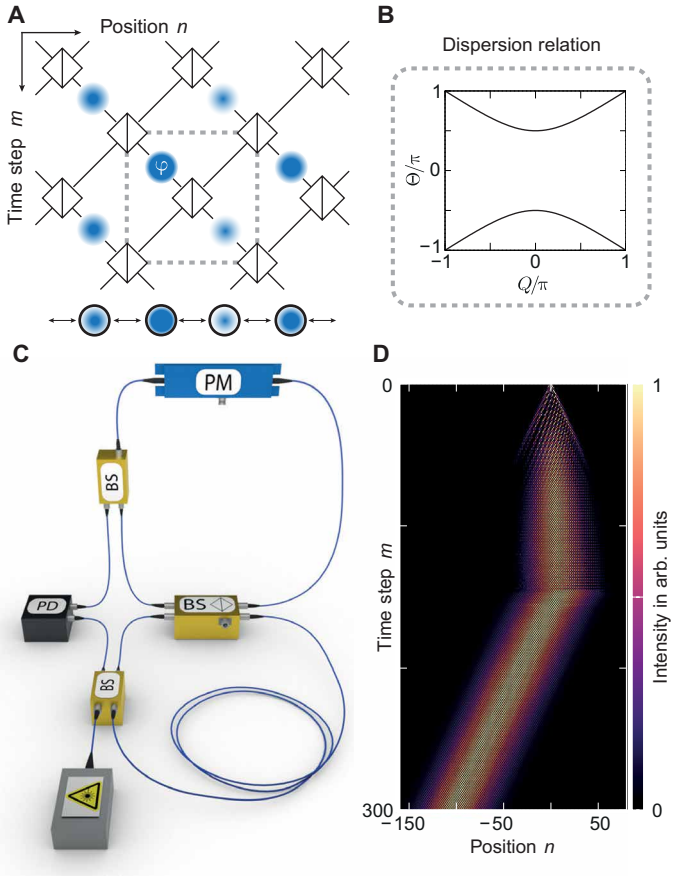

Fig. 3. Synthetic photonic lattices and experimental setup. (**A**) Double-discrete synthetic photonic lattice consisting of a mesh of beam splitters and its equivalent 1D chain of sites. Phase modulation φ_u of spatially random distribution (blue circles with strength varying in n) corresponds to a disordered on-site potential of the chain. (**B**) Dispersion relation of the disorder-free homogeneous photonic lattice, where Q corresponds to the quasi-momentum and Θ to the quasi-energy (propagation constant), respectively. (**C**) Experimental setup (simplified) consisting of two optical fiber loops, one shorter than the other, coupled by a beam splitter (BS). A laser pulse is injected into the loops. The pulse propagation in the loops can be mapped onto a 1 + 1D double-discrete lattice shown in (A). The pulse intensities are measured with a photodetector (PD). A phase modulator (PM) shapes the real part of the lattice potential. (**D**) Experimental data showing the creation of a Gaussian wave packet to excite $Q = 0.8\pi$ in the upper band of the dispersion relation. Starting from a single pulse, a discrete diffraction pattern is formed and manipulated to reach a Gaussian shape with a defined momentum (time steps $m = 1 \ldots 155$). From $m = 156$, the Gaussian beam of width $n_w = 30$ with a mean momentum of $Q = 0.8\pi$ propagates in the homogeneous (disorder-free) Hermitian lattice.

the optical fiber loops. The reason for this is that the differences in the intensity distributions between the short and the long loop are only on local scales, which vanish in the averaging process. The experimental data and the corresponding simulations are therefore based on the pulse intensities $|u_n^m|^2$ of the shorter loop.

To evaluate the first- and second-order scattering processes, we derive the dispersion relation for the disorder-free system. For a uniform time-independent potential, $\varphi_u(n, m) = \varphi_0 \in \mathbb{R}$, we introduce the Floquet-Bloch ansatz to deduce the dispersion relation $2\cos(\Theta) = \cos(Q) - 1$, with solutions of the form $u_n^m = U(Q,\Theta)\,e^{iQn/2}\,e^{-i\Theta m/2}$ and $v_n^m = V(Q,\Theta)\,e^{iQn/2}\,e^{-i\Theta m/2}$ (Fig. 3B). Each plane wave solution is

characterized by a Bloch momentum $Q \in [-\pi, \pi]$ and a propagation constant $\Theta \in [-\pi, \pi]$ (corresponding to k and β, respectively, in Eqs. 1 and 2). Typically, in this system, wave packets in the vicinity of $Q = \pm\pi$ have the highest group velocity but the lowest group velocity dispersion, whereas wave packets with the lowest momentum $Q \approx 0$ experience low group velocity but the highest dispersion.

Since we are interested here in studying the propagation of wave packets in different spectral regions (corresponding to Fig. 2), we excite a spectrally narrow region by creating a spatially broad Gaussian beam $u_n = \exp(-n^2/2n_w^2)\exp(-iQn/2)$, with $n_w = 30$, launched with a controlled central momentum Q. The generation of the Gaussian beam relies on a non-Hermitian diffusion process (*52*), allowing to maintain an extremely stable phase relation between the optical pulses (see details in the fifth section of the Supplementary Materials). The experimental results (Fig. 3D) show the sequential buildup of the Gaussian beam (time steps $m \leq 155$) and, subsequently, its free propagation in a homogeneous system ($\varphi_u = 0$) at time steps $m > 155$, for the specific example of $Q = 0.8\pi$. The propagation of this synthetically constructed Gaussian wave packet displays the width expansion and tilt angle (Fig. 3D), which, in the absence of any disorder, coincide with the diffraction broadening akin to propagation in homogeneous linear media.

To study the effects of disorder in our synthetic lattice, it is essential to explain that the phase the pulses accumulate, φ_u, is analogous to the phase accumulated by passing through a potential term in Schrödinger's equation. For example, a phase $\varphi_u(n, m) = \sin(Q_0 n)$ is equivalent to a periodic single-frequency (sinusoidal) potential that scatters a plane wave with wave number Q to a plane wave with $Q + Q_0$. As in almost every scattering process, here too, first-order transitions dominate the process, but in principle, two-step transitions, e.g., $-Q_0 \xrightarrow{+Q_0} 0$ followed by a second transition $0 \xrightarrow{+Q_0} Q_0$, are also possible because the overall transition conserves the quasi-energy Θ (analogous to the longitudinal momentum in Eqs. 1 and 2). The efficiency of these second-order transitions is, here too, usually low because $Q = 0$ is a virtual level. This makes it

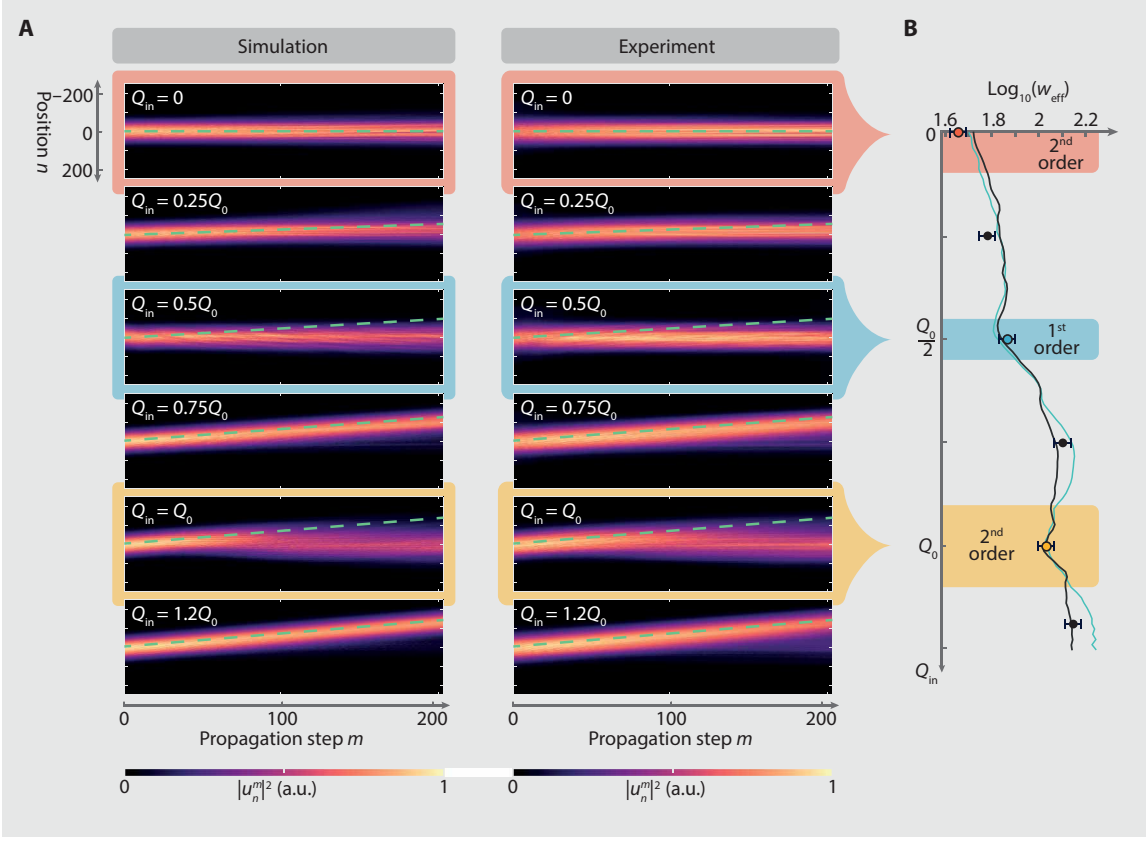

Fig. 4. Experimental observation of localization outside the spectral extent of the disorder. (**A**) Simulated and experimentally measured ensemble-averaged propagation, taken over 100 disorder realizations with $A_{DS} = 0.4$, for a Gaussian wave packet with width $n_w = 50$ launched at various initial momenta Q_{in}. The green lines mark the beam trajectory in the absence of disorder. At $Q_{in} = 0$, the wave packet evolves without expanding due to second-order processes combined with the weak diffraction broadening. At $Q_{in} = 0.25Q_0$, the wave packet is within the spectral extent of the disorder and therefore localizes. For $Q_{in} = 0.5Q_0$, multiple first-order transitions are phase matched; hence, the wave packet localizes: It evolves to on-axis propagation and stops expanding. For $Q_{in} = 0.75Q_0$, the transitions are energy mismatched, so the wave packet continues on its initial trajectory and expands, as if it was unaffected by the disorder. At $Q_{in} = Q_0$, we find evolution in the regime of strictly second-order localization processes. Initially, the wave packet expands, but after some distance, the expansion stops, and the beam propagates on axis. For $Q_{in} = 1.2Q_0$, the transitions are again phase mismatched, so the wave packet is unaffected by the disorder. (**B**) Effective width versus initial quasi-momentum Q at the end of the propagation, showing local minima exactly in the first-order (blue) and second-order localization (red and orange) regions. The measured values [circles with error bars (SD)] qualitatively agree with the theoretical calculation (black). The blue curve stands for simulated results of a larger lattice ($N = 1000$) with longer evolution time ($m = 300$) and a larger initial width ($n_w = 80$) (beyond reach of our experiments), underlining the main trends found in the experiments.

clear why Anderson localization via these second-order transitions has thus far never been observed.

We now proceed to implement the bandwidth-limited disordered potential as described above (Fig. 1B) in our synthetic lattice. First, the potential has to be evolution invariant; otherwise, if the potential varies throughout propagation, the beam will undergo diffusion or hyper-transport but not localization (*20*). To do that, we choose a random potential $\varphi_u(n)$ that is constant with every time step m. We generate the disorder to have the power spectrum $S_\varphi(Q) = |\mathrm{FT}\{\varphi_u(n)\}|^2$ comprising many spectral components with random amplitude and phase, all restricted to a small region around some frequency Q_0. The spectrum of the disordered potential is nonzero only around $Q_0 = \pm 0.4\pi$ with width $\Delta Q_0 \simeq 0.2\,|Q_0|$ (similar to k_0 and Δk in Fig. 1B). Last, we launch a broad Gaussian beam ($n_w = 50$) with a central momentum Q into the disordered synthetic lattice. Figure 4A presents the calculated and measured ensemble-average squared modulus of the wave function. The average is taken over 100 experiments, each for a different realization of the disorder, with the same (nonzero) range of $S_\varphi(Q)$ and the same disorder strength, $A_{DS} = 0.4$, defined by $A_{DS} = \sqrt{\Sigma_n \varphi_u(n)^2}\Big/\frac{N}{2}$. We repeat this experiment for several initial momenta Q of the Gaussian beam, which is equivalent to several angles of incidence in the transverse localization scheme of Eq. 1.

Figure 4 shows the ensemble-averaged intensity as it evolves in the disordered synthetic lattice. We examine the trajectories of the ensemble-averaged beams and search for the hallmark feature of Anderson localization: localized wave packets that come to a halt irrespective of their initial momentum. We find that for certain Q values, the beams maintain their initial trajectories and exhibit diffraction broadening, unaffected by localization processes, as if there is no disorder, whereas beams with other Q values change their initial trajectories to propagate parallel to the time step axis (zero transverse velocity), irrespective of their initial momentum, and stop expanding in their width (Fig. 4A). These latter Q values correspond to localization by first-order transitions at $Q = 0.5Q_0$ (more efficient transitions, narrower localized beam) and by second-order transition at $Q = Q_0$ (less efficient, broader beam). The dominant process that causes this type of localization is a series of symmetric scatterings to virtual states and back, which naturally occurs in any Hermitian system. We find that localization by strictly small-scale disorder (smaller than the wavelength of the wave packet) takes a larger propagation distance to set in (see the fifth section in the Supplementary Materials); hence, the losses should be minimized for observing this phenomenon in experiments. In addition, we also find localization at $Q_{in} = 0.25Q_0$, which occurs by the process of bandwidth expansion due to strong disorder (see the discussion in the fourth section of the Supplementary Materials). On the other hand, we find that at other Q values, e.g., $Q_{in} = 0.75Q_0$ and $1.2Q_0$, the beam has almost no interaction with the disordered potential and continues on its initial trajectory undergoing nearly free diffraction, as if the underlying lattice was disorder free.

Next, we extract the effective width for each initial momentum (Fig. 4B), after a large propagation time in the system. The effective width displays several local minima around initial momenta 0, $Q_0/2$, and Q_0, which serves as a direct indication for Anderson localization, and conforms with the respective theoretical plot in Fig. 2B (calculated for the transverse localization scheme of Eq. 1). Here, similar to Fig. 2B, although second-order processes are generally weak, the low group velocities of low wave numbers ($Q_{in} \sim 0$) can generally lead to stronger localization and therefore to lower w_{eff}, with localization as strong as first-order localization. The zero transverse velocity and the decreased diffraction broadening for $Q_{in} = Q_0$, displayed in Fig. 4, are direct experimental evidence for localization outside the spectral extent of the disorder.

Last, we study the exponential decay characterizing the ensemble-averaged wave packet localized through second-order transitions. We do that by extracting the spatial intensity distribution (after large propagation times) from the experimental data and comparing to those of "ordinary" (first-order) localization. Figure 5 shows the characteristic exponential decay of the ensemble-average wave packets, at $Q = 0$, at $Q_0/2$, and at Q_0, respectively.

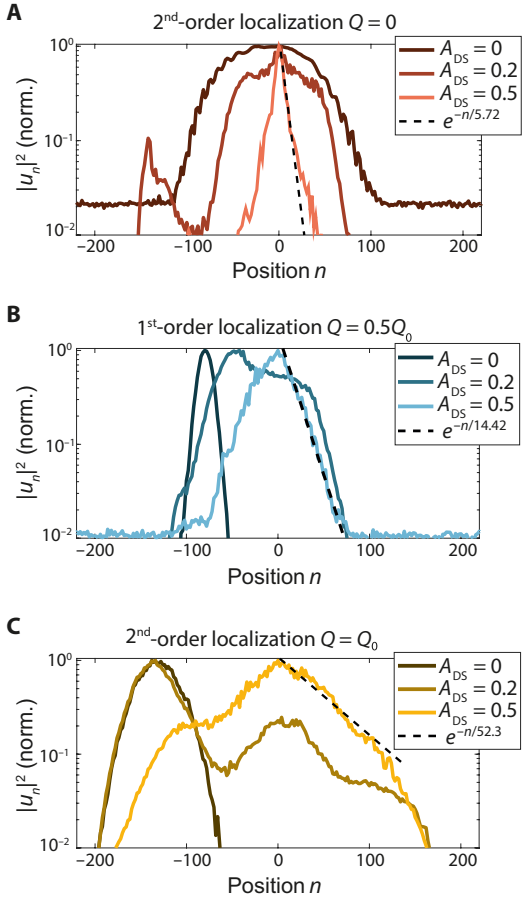

Fig. 5. Experimental signatures of Anderson localization inside and outside the spectral extent of the disorder. (**A** to **C**) Shape of the ensemble-averaged wave packet, taken over 100 disorder realizations, after propagating 200 time steps in the synthetic photonic lattice with bandwidth-limited disorder, each for three different values of disorder strength, A_{DS}, ranging from zero to strong disorder. The initial widths of the wave packets for $Q = 0, 0.5Q_0, Q_0$ are $n_w = 3.5, 10, 30$, respectively. As the disorder is made stronger, the wave functions become localized and exhibit exponential decay. This happens not only at $Q = 0.5Q_0$ by first-order processes (B) but also at $Q = 0$ (A) and at $Q = Q_0$ (C), where localization stems strictly from second-order processes. For strong disorder, all wave packets are exponentially localized and are centered on the initial site $n = 0$, irrespective of their initial momentum. We extract the localization length in all cases and find it to be at least an order of magnitude smaller than the system size ($n = -200 \ldots 200$). The slightly different baselines stem from different optical noise levels in the different experimental runs.

For each initial Q, we use a suitable width for the initial wave packet to excite a minimal number of localized modes in each regime (i.e., a too wide initial beam might excite many narrow localized modes, so that the shape of the propagating wave packet would remain similar to the input beam). As the disorder is made stronger, the localized wave functions become narrower and acquire an exponential shape despite some asymmetry present due to their initial nonzero group velocity. This happens not only at $Q_0/2$ (first-order localization) but also at $Q_{in} = 0$ and $Q_{in} = Q_0$, where localization is strictly by second-order localization processes. At the strongest disorder, all wave packets are exponentially localized and are all centered on $n = 0$ (effectively zero transverse velocity), irrespective of their initial momentum. We extract the localization length and find that, in all cases, it is at least an order of magnitude smaller than the system size, assuring that all the effects observed are not affected by the system size. Moreover, this length is found to be shorter for lower initial quasi-momenta due to their low group velocities.

DISCUSSION

In conclusion, we presented the first experiments showing Anderson localization completely outside the spectral extent of the disorder, both at very low and at very high wave numbers. The localization at low wave numbers is especially intriguing: It implies that localization can also occur at low wave numbers, even when the spectrum of the disorder is strictly at high wave numbers. This feature is universal, arising from the symmetry of the power spectrum of the disorder, and it is therefore expected to occur for any Hermitian system. This feature may also apply to non-Hermitian systems, but non-Hermiticity can break the symmetry of $|V(k)|$, so we leave this topic to future studies. Overall, the phenomenon of localization by higher-order scattering processes implies that even if a system is highly correlated [e.g., amorphous structures (*22*, *53*–*55*) or hyperuniform materials (*56*)], waves of any wave number, even those beyond the disorder spectrum, can experience Anderson localization. In this vein, it should be possible to observe short localization lengths induced strictly by third-order transitions or higher. We anticipate that new mobility edges would be induced by virtual transitions in 2D and 3D and also in higher dimensions that include disorder in synthetic space (*32*). Our results expand the understanding of disordered systems and suggest developing the notion of bandwidth-limited disorder for controlling the localization and transport in desired spectral ranges.

MATERIALS AND METHODS

Experimental implementation

In this section, we briefly describe the experimental setup. The setup consists of two optical fiber loops, coupled by a beam splitter as shown in Fig. 3C. For technical reasons, in each fiber loop, additional optical components are incorporated. Each loop contains a spool of a single-mode fiber (Corning Vascade LEAF EP) to extend the round-trip time to approximately 30 μs. By adding a standard single-mode fiber patch cord into the u loop, we create a difference in the round-trip time between the loops of approximately 100 ns. We use an optical fiber coupler (AC Photonics) to couple the photodetector (1.2-GHz indium gallium arsenide) and the seed pulse injection (see Fig. 3C). The seed pulse generation is based on a continuous wave distributed feedback (DFB) laser diode (JDS Uniphase, 2-MHz linewidth, 1550-nm center), where a rectangular 40- to 60-ns pulse is cut out via intensity modulation. The intensity modulation relies on a Mach-Zehnder intensity modulator (SDL Integrated Optics Limited) and an acousto-optical modulator (Brimrose Corp.). To maintain a high signal-to-noise ratio, we use erbium-doped fiber amplifiers (EDFAs; from Thorlabs), which are optically gain-clamped by a continuous wave DFB laser diode at 1538 nm. This pilot laser is inserted into the amplifier via wavelength division multiplexing couplers (AC Photonics) and afterward removed using an optical bandpass filter (WL Photonics). The filters also drastically reduce the level of amplified spontaneous emission originating from the EDFAs. In this way, a sufficiently high signal-to-noise ratio can be maintained throughout the used number of time steps. We set the peak power of the pulses to be low enough to avoid effects of gain saturation, which can serve as undesired nonlinearities in this experiment. However, we also maintain a signal that is strong enough to be dominant despite the noise created by amplified spontaneous emission from the EDFAs. To incorporate gain and loss for the preparation of the synthetic Gaussian beam, we place an acousto-optical intensity modulator in each loop. The output of the modulators is aligned to the 0th diffraction order to avoid frequency shifts. The working point of the modulators is set to a value between 0 and 1. The amplifiers compensate the overall round-trip losses in this setting. By varying the transmission of the intensity modulator, one can effectively achieve gain or loss. The beam splitter connecting the fiber loops is a variable fiber optical coupler (Agiltron Inc.) that can electronically control the coupling between the two loops. We use a phase modulator (iXBlue Phot.) to control the phase of the pulses and therefore the real part of the analog lattice potential. In addition, we use a polarization controller (Thorlabs) for aligning the correct polarization for the $LiNbO_3$-based components. The waveforms of the modulators are prepared with MATLAB and generated with arbitrary waveform generators (Keysight Tech.). For the data acquisition, the output voltages of the photodetectors are amplified (FEMTO HLVA-100) and then sampled with an oscilloscope (Rohde & Schwarz). The basis time scales T and Δt, which are required for mapping the pulse intensities on the 1 + 1D lattice, are extracted from a control experiment in a homogeneous lattice with a single-site excitation. Last, we apply a baseline correction to the experimental data, which filters out the optical noise floor.

SUPPLEMENTARY MATERIALS

Supplementary material for this article is available at https://science.org/doi/10.1126/sciadv.abn7769

REFERENCES AND NOTES

1. Titus Lucretius Carus, *De rerum natura ("On the nature of things"), circa 60BC*.
2. P. Drude, *Zur Elektronentheorie der Metalle. Ann. Phys.* **306**, 566–613 (1900).
3. P. W. Anderson, Absence of diffusion in certain random lattices. *Phys. Rev. Lett.* **109**, 1492 (1958).
4. S. S. Abdullaev, G. M. Zaslavskii, Nonlinear dynamics of rays in inhomogeneous media. *Zhurnal Eksp. i Teor. Fiz.* **80**, 524–536 (1981).
5. C. H. Hodges, Confinement of vibration by structural irregularity. *J. Sound Vib.* **82**, 411–424 (1982).
6. S. John, Electromagnetic absorption in a disordered medium near a photon mobility edge. *Phys. Rev. Lett.* **53**, 2169–2172 (1984).
7. H. De Raedt, A. Lagendijk, P. de Vries, Transverse localization of light. *Phys. Rev. Lett.* **62**, 2–5 (1989).
8. D. S. Wiersma, P. Bartolini, A. Lagendijk, R. Righini, Localization of light in a disordered medium. *Nature* **390**, 671–673 (1997).
9. M. V. Berry, S. Klein, Transparent mirrors: Rays, waves and localization. *Eur. J. Phys.* **18**, 222–228 (1997).

10. M. Störzer, P. Gross, C. M. Aegerter, G. Maret, Observation of the critical regime near anderson localization of light. *Phys. Rev. Lett.* **96**, 063904 (2006).
11. A. A. Chabanov, M. Stoytchev, A. Z. Genack, Statistical signatures of photon localization. *Nature* **404**, 850–853 (2000).
12. U. Kuhl, F. M. Izrailev, A. A. Krokhin, H. J. Stöckmann, Experimental observation of the mobility edge in a waveguide with correlated disorder. *Appl. Phys. Lett.* **77**, 633–635 (2000).
13. T. Schwartz, G. Bartal, S. Fishman, M. Segev, Transport and Anderson localization in disordered two-dimensional photonic lattices. *Nature* **446**, 52–55 (2007).
14. Y. Lahini, A. Avidan, F. Pozzi, M. Sorel, R. Morandotti, D. N. Christodoulides, Y. Silberberg, Anderson localization and nonlinearity in one-dimensional disordered photonic lattices. *Phys. Rev. Lett.* **100**, 013906 (2008).
15. S. Karbasi, R. J. Frazier, K. W. Koch, T. Hawkins, J. Ballato, A. Mafi, Image transport through a disordered optical fibre mediated by transverse Anderson localization. *Nat. Commun.* **5**, 1–9 (2014).
16. H. Hu, A. Strybulevych, J. H. Page, S. E. Skipetrov, B. A. van Tiggelen, Localization of ultrasound in a three-dimensional elastic network. *Nat. Phys.* **4**, 945–948 (2008).
17. J. Billy, V. Josse, Z. Zuo, A. Bernard, B. Hambrecht, P. Lugan, D. Clément, L. S.-Palencia, P. Bouyer, A. Aspect, Direct observation of Anderson localization of matter waves in a controlled disorder. *Nature* **453**, 891–894 (2008).
18. G. Roati, C. D'Errico, L. Fallani, M. Fattori, C. Fort, M. Zaccanti, G. Modugno, M. Modugno, M. Inguscio, Anderson localization of a non-interacting Bose–Einstein condensate. *Nature* **453**, 895–898 (2008).
19. P. Barthelemy, J. Bertolotti, D. S. Wiersma, A Lévy flight for light. *Nature* **453**, 495–498 (2008).
20. L. Levi, Y. Krivolapov, S. Fishman, M. Segev, Hyper-transport of light and stochastic acceleration by evolving disorder. *Nat. Phys.* **8**, 912–917 (2012).
21. H. H. Sheinfux, Y. Lumer, G. Ankonina, A. Z. Genack, G. Bartal, M. Segev, Observation of Anderson localization in disordered nanophotonic structures. *Science* **356**, 953–956 (2017).
22. M. Rechtsman, A. Szameit, F. Dreisow, M. Heinrich, R. Keil, S. Nolte, M. Segev, Amorphous photonic lattices: Band gaps, effective mass, and suppressed transport. *Phys. Rev. Lett.* **106**, 193904 (2011).
23. J. Haberko, L. S. Froufe-Pérez, F. Scheffold, Transition from light diffusion to localization in three-dimensional amorphous dielectric networks near the band edge. *Nat. Commun.* **11**, 1–9 (2020).
24. P. Wang, Y. Zheng, X. Chen, C. Huang, Y. V. Kartashov, L. Torner, V. V. Konotop, F. Ye, Localization and delocalization of light in photonic moiré lattices. *Nature* **557**, 42–46 (2020).
25. A. F. Tzortzakakis, K. G. Makris, E. N. Economou, Non-Hermitian disorder in two-dimensional optical lattices. *Phys. Rev. B.* **101**, 014202 (2020).
26. E. Abrahams, P. W. Anderson, D. C. Licciardello, T. V. Ramakrishnan, Scaling theory of localization: Absence of quantum diffusion in two dimensions. *Phys. Rev. Lett.* **42**, 673–676 (1979).
27. I. M. Lifshits, S. A. Gredeskul, L. A. Pastur, *Introduction to the Theory of Disordered Systems* (Wiley, 1988).
28. D. H. Dunlap, H. L. Wu, P. W. Phillips, Absence of localization in a random-dimer model. *Phys. Rev. Lett.* **65**, 88–91 (1990).
29. F. M. Izrailev, A. A. Krokhin, Localization and the mobility edge in one-dimensional potentials with correlated disorder. *Phys. Rev. Lett.* **82**, 4062–4065 (1999).
30. Y. Lahini, Y. Bromberg, Y. Shechtman, A. Szameit, D. N. Christodoulides, R. Morandotti, Y. Silberberg, Anderson localization in optiacal waveguide arrays with off diagonal coupling disorder. *Phys. Rev. A - At. Mol. Opt. Phys.* **84**, 13636–13646 (2011).
31. M. Segev, Y. Silberberg, D. N. Christodoulides, Anderson localization of light. *Nat. Photonics.* **7**, 197–204 (2013).
32. E. Lustig, M. Segev, Topological photonics in synthetic dimensions. *Adv. Opt. Photon.* **13**, 426–461 (2021).
33. A. Schreiber, K. N. Cassemiro, V. Potoček, A. Gábris, I. Jex, C. H. Silberhorn, Decoherence and disorder in quantum walks: From ballistic spread to localization. *Phys. Rev. Lett.* **106**, 180403 (2011).
34. S. John, M. J. Stephen, Wave propagation and localization in a long-range correlated random potential. *Phys. Rev. B.* **28**, 6358–6368 (1983).
35. J. C. Flores, Transport in models with correlated diagonal and off-diagonal disorder. *J. Phys. Condens. Matter* **1**, 8471–8479 (1989).
36. G. Samelsohn, S. A. Gredeskul, R. Mazar, Resonances and localization of classical waves in random systems with correlated disorder. *Phys. Rev. E.* **60**, 6081–6090 (1999).
37. E. Gurevich, O. Kenneth, Lyapunov exponent for the laser speckle potential: A weak disorder expansion. *Phys. Rev. A* **79**, 063617 (2009).
38. V. Bellani, E. Diez, R. Hey, L. Toni, L. Tarricone, G. B. Parravicini, F. Domínguez-Adame, R. Gómez-Alcalá, Experimental evidence of delocalized states in random dimer superlattices. *Phys. Rev. Lett.* **82**, 2159–2162 (1999).
39. P. Lugan, A. Aspect, L. Sanchez-Palencia, D. Delande, B. Grémaud, C. A. Müller, C. Miniatura, One-dimensional Anderson localization in certain correlated random potentials. *Phys. Rev. A* **80**, 023605 (2009).
40. A. Dikopoltsev, H. Herzig Sheinfux, M. Segev, Localization by virtual transitions in correlated disorder. *Phys. Rev. B.* **100**, 140202 (2019).
41. M. C. Rechtsman, J. M. Zeuner, Y. Plotnik, Y. Lumer, D. Podolsky, F. Dreisow, S. Nolte, M. Segev, A. Szameit, Photonic Floquet topological insulators. *Nature* **496**, 196–200 (2013).
42. Y. Plotnik, O. Peleg, F. Dreisow, M. Heinrich, S. Nolte, A. Szameit, M. Segev, Experimental observation of optical bound states in the continuum. *Phys. Rev. Lett.* **107**, 183901 (2011).
43. S. Stützer, Y. Plotnik, Y. Lumer, P. Titum, N. H. Lindner, M. Segev, M. C. Rechtsman, A. Szameit, Photonic topological Anderson insulators. *Nature* **560**, 461–465 (2018).
44. A. Yariv, Coupled-mode theory for guided-wave optics. *IEEE J. Quantum Electron.* **9**, 919–933 (1973).
45. A. Schreiber, K. N. Cassemiro, V. Potoček, A. Gábris, P. J. Mosley, E. Andersson, I. Jex, C. Silberhorn, Photons walking the line: A quantum walk with adjustable coin operations. *Phys. Rev. Lett.* **104**, 050502 (2010).
46. A. Regensburger, C. Bersch, M. A. Miri, G. Onishchukov, D. N. Christodoulides, U. Peschel, Parity-time synthetic photonic lattices. *Nature* **488**, 167–171 (2012).
47. M. Wimmer, M. A. Miri, D. Christodoulides, U. Peschel, Observation of Bloch oscillations in complex PT-symmetric photonic lattices. *Sci. Rep.* **5**, 1–8 (2015).
48. M. Wimmer, A. Regensburger, M. A. Miri, C. Bersch, D. N. Christodoulides, U. Peschel, Observation of optical solitons in PT-symmetric lattices. *Nat. Commun.* **6**, 1–9 (2015).
49. A. L. M. Muniz, M. Wimmer, A. Bisianov, U. Peschel, R. Morandotti, P. S. Jung, D. N. Christodoulides, 2D solitons in PT-symmetric photonic lattices. *Phys. Rev. Lett.* **123**, 253903 (2019).
50. M. Wimmer, H. M. Price, I. Carusotto, U. Peschel, Experimental measurement of the Berry curvature from anomalous transport. *Nat. Phys.* **13**, 545–550 (2017).
51. S. Weidemann, M. Kremer, T. Helbig, T. Hofmann, A. Stegmaier, M. Greiter, R. Thomale, A. Szameit, Topological funneling of light. *Science* **368**, 311–314 (2020).
52. T. Eichelkraut, R. Heilmann, S. Weimann, S. Stützer, F. Dreisow, D. N. Christodoulides, S. Nolte, A. Szameit, Mobility transition from ballistic to diffusive transport in non-Hermitian lattices. *Nat. Commun.* **4**, 1–7 (2013).
53. C. Jin, X. Meng, B. Cheng, Z. Li, D. Zhang, Photonic gap in amorphous photonic materials. *Phys. Rev. B.* **63**, 195107 (2001).
54. N. P. Mitchell, L. M. Nash, D. Hexner, A. M. Turner, W. T. M. Irvine, Amorphous topological insulators constructed from random point sets. *Nat. Phys.* **14**, 380–385 (2018).
55. P. Zhou, G. G. Liu, X. Ren, Y. Yang, H. Xue, L. Bi, L. Deng, Y. Chong, B. Zhang, Photonic amorphous topological insulator. *Light Sci. Appl.* **9**, 1–8 (2020).
56. O. Leseur, R. Pierrat, R. Carminati, High-density hyperuniform materials can be transparent. *Optica.* **3**, 763 (2016).
57. G. J. Aubry, L. S. Froufe-Pérez, U. Kuhl, O. Legrand, F. Scheffold, F. Mortessagne, Experimental tuning of transport regimes in hyperuniform disordered photonic materials. *Phys. Rev. Lett.* **125**, 127402 (2020).
58. D. J. Thouless, Anderson's theory of localized states. *J. Phys. C Solid State Phys.* **3**, 1559 (1970).
59. I. M. Lifshits, S. A. Gredeskul, L. A. Pastur, *Introduction to the Theory of Disordered Systems* (Wiley-VCH, 1988).
60. M. Wimmer, A. Regensburger, C. Bersch, M.-A. Miri, S. Batz, G. Onishchukov, D. N. Christodoulides, U. Peschel, Optical diametric drive acceleration through action–reaction symmetry breaking. *Nat. Phys.* **9**, 780–784 (2013).

Acknowledgments

Funding: M.S. and A.Sz. acknowledge the support of a DIP research grant by the German-Israeli Science Foundation. **Author contributions:** A.D., S.W., and M.K. contributed equally to this work as first authors. All authors contributed significantly to this work. **Competing interests:** The authors declare that they have no competing interests. **Data and materials availability:** All data needed to evaluate the conclusions in the paper are present in the paper and/or the Supplementary Materials and at https://doi.org/10.18453/rosdok_id00003518. Supplementary information is available for this paper. The supplementary information contains explanations on the equivalence between the paraxial wave equation and the Schrödinger equation, the method we used to design the disorder in the spectral domain, the effect of increased spectral extent in strong and correlated disorder, effective width calculation in disordered systems, the implementation of the time-bin–encoded photonic lattice we use as an experimental platform, and the method we use to create a Gaussian beam in such a lattice. Correspondence and requests for materials should be addressed to alexander.szameit@uni-rostock.de.

Submitted 20 December 2021
Accepted 8 April 2022
Published 25 May 2022
10.1126/sciadv.abn7769

ScienceAdvances

Observation of Anderson localization beyond the spectrum of the disorder

Alex DikopoltsevSebastian WeidemannMark KremerAndrea SteinfurthHanan Herzig SheinfuxAlexander SzameitMordechai Segev

Sci. Adv., 8 (21), eabn7769. • DOI: 10.1126/sciadv.abn7769

Science Advances (ISSN) is published by the American Association for the Advancement of Science. 1200 New York Avenue NW, Washington, DC 20005. The title *Science Advances* is a registered trademark of AAAS.